RSC Advances

PAPER

View Article Online
View Journal | View Issue

Cite this: *RSC Adv.*, 2024, **14**, 36733

Enhanced desulfurization performance of model fuel by Cu–ZnO/TiO_2 heterostructure†

Jiaxin Xu, Yongjie Zheng, * Jingzhi Tian, Yunpeng Zhao and Heshan Zheng

Received 22nd September 2024
Accepted 7th November 2024

DOI: 10.1039/d4ra06833e

rsc.li/rsc-advances

A facile hydrothermal approach was employed to synthesize a novel Cu–ZnO/TiO_2 Z-heterojunction with a high density of defects, which was then utilized for the oxidative desulfurization process, demonstrating excellent photodegradation performance. The results showed that by adjusting components such as Cu, ZnO, and TiO_2, the removal efficiency of DBT reached 88.12% within a duration of 240 min. In the 5 repeated experiments, 7.5%Cu–ZnO/TiO_2 still exhibited high stability and could be reused. The improved photocatalytic performance of the 7.5%Cu–ZnO/TiO_2 composite can be attributed to its high light absorption capability and well-matched energy levels, which are due to the abundant presence of imperfections. The adoption of a Z-heterojunction has enabled efficient separation and transfer of photo-generated electrons and holes (e^-/h^+), thereby reducing the probability of charge carrier recombination.

1 Introduction

In the combustion process of automobile engines, due to the oxidation reaction of organic sulfide, a large amount of SO_X is produced, which is the main cause of acid rain. As a result, environmental concerns have compelled refiners to develop effective desulfurization technologies for the removal of these sulfur-containing compounds. HDS is commonly used for industrial desulfurization, but it faces challenges in removing organic sulfides with steric hindrance.[1,2] PODS is a cost-effective and efficient method for desulfurization that eliminates the need for hydrogen gas, while also exhibiting high oxidative activity towards difficult-to-dissolve sulfur compounds like dibenzothiophene (DBT).

The wide band gap and limited utilization of visible light of TiO_2 and ZnO affect their overall efficiency.[3–5] Therefore, people have been focusing on improving the activity of photocatalyst through morphological regulation, metal or non-metal doping, defect engineering, *etc.*[6–10] In particular, heterojunction construction with other semiconductors with advantages in bandgap and photocatalytic activity can effectively promote photogenerated charge transfer, inhibit carrier recombination, and improve light utilization efficiency. Since the conduction potential and valence band potential of ZnO are slightly lower than those of TiO_2, when ZnO and TiO_2 form a type II heterojunction, charge can be effectively transferred from ZnO to TiO_2.[11] Additionally, hole transfer occurs in the opposite direction, which aids in achieving efficient electron–hole separation.[12–14] The ZnO–TiO_2 composite nanomaterials were synthesized using the co-precipitation method, as reported by Lachom *et al.*[15] The reaction rate constant of methyl orange was found to be 1.86×10^{-2} min^{-1}, demonstrating a significant improvement in efficiency compared to pure TiO_2 and ZnO particles. Cheng *et al.* selectively deposited amorphous TiO_2 onto the tips of ZnO nanorods, resulting in a ZnO/TiO_2 hybrid nanostructure leads to the manifestation of remarkably improved photocatalytic performance in comparison to that of individual ZnO nanorods and amorphous TiO_2 nanoparticles.[16] Song *et al.* discovered that ZnO nanorods were grafted onto electrospun TiO_2 nanofibers using hydrothermal technology, and silver metal nanoparticles were uniformly dispersed on the surface to create a ternary photocatalyst.[17] The presence of the heterostructure and Schottky barrier significantly enhances the photocatalytic activity, thereby effectively improving the antibiotic effect.

Anatase type TiO_2 has higher reactivity on the (001) crystal surface, but at present most crystals are mainly exposed on the (101) surface, which has lower surface energy. By employing titanium tetrafluoride as the primary ingredient and HF as the regulating agent, Yang *et al.* effectively produced anatase TiO_2 with a surface exposure percentage of 47% on the (001) plane.[18] However, the catalysis of fluoride makes the photocatalyst highly toxic and corrosive, and it is difficult to remove fluorine-containing compounds. Zhao *et al.* synthesized a stable mesoporous anatase type TiO_2 nanosphere by hydrothermal method, and effectively stabilized the (001) plane by using sulfuric acid as an inducer and capping agent.[19] The interaction between sulfuric acid and the (001) plane exhibits a relatively weak affinity, which facilitates the easy removal of the sulfuric acid capping agent through washing.

Qiqihar University, Qiqihar 161006, P. R. China. E-mail: zyj1964@163.com; Fax: +86-452-2738152

† Electronic supplementary information (ESI) available. See DOI: https://doi.org/10.1039/d4ra06833e

The paper successfully synthesized anatase TiO_2 nanospheres with a (001) crystal surface without fluorine, and grafted ZnO nanoneedles onto the surface to construct a photocatalytic material with ternary Z-type heterojunction. The photocatalytic activity of (Cu–ZnO/TiO_2) was evaluated, and its stability and repeatability were verified through systematic studies of chemical composition, structure, morphology, and physicochemical properties. Additionally, free radical trapping experiments were conducted to explore the possible photocatalytic mechanism.

2 Experiment

2.1 Materials and chemical reagents

Tetrabutyl titanate (TBOT, 98.0%) and zinc acetate (99.0%) are offered by Tianjin Kemi Ou Chemical Reagent Co., Ltd. The copper nitrate (99.0%) is provided by Tianjin Guangfu Fine Chemical Research Institute. Sodium hydroxide (96.0%) is provided by Tianjin Damao Chemical Reagent Factory. Sulfuric acid (98.0%) is provided by Liaoning Quanrui Reagent Co., Ltd. The dibenzothiophene (DBT, 99.0%), benzothiophene (BT, 99.0%), thiophene (T, 99.0%), and *n*-octane (96.0%) are from Shanghai Maclin Biochemical Technology Co., Ltd. Anhydrous ethanol (99.8%) is provided by Tianjin Kai Tong Chemical Reagent Co., Ltd.

2.2 Synthesis of materials

2.2.1 Preparation of anatase TiO_2 microspheres. The synthesis of anatase TiO_2 spheres was achieved using a simple hydrothermal technique. Initially, a 1.5 ml solution of titanium butoxide (TBOT) was introduced into a 100 ml mixture containing sulfuric acid (H_2SO_4) at a concentration of 2.2 M, followed by stirring for a duration of 30 minutes. Following this, the suspension mentioned earlier was introduced into a Teflon-lined stainless steel autoclave with a volume of 100 ml and subjected to a reaction at a temperature of 180 °C for a duration of 12 hours. After allowing the mixture to cool naturally to ambient temperature, the solid was isolated by centrifugation and then washed with deionized water and anhydrous ethanol until it reached a pH level of neutrality. Subsequently, it was then dried in an oven.

2.2.2 Preparation of ZnO/TiO_2 and Cu–ZnO/TiO_2 composite materials. Preparation of ZnO/TiO_2 composite materials: to begin with, a solution referred to as solution A was prepared by dispersing 0.5 g of TiO_2 in 20 ml of deionized water. The B solution is composed of zinc acetate, sodium hydroxide, and 30 ml of distilled water. After undergoing ultrasonic dispersion, the A solution is slowly mixed with the B solution in a dropwise manner. The obtained suspension was subsequently stirred using a mechanical stirrer for 30 min and then transferred into a high-pressure stainless steel reactor with a capacity of 100 ml for a crystallization reaction at 160 °C over a period of 24 hours. The ZnO/TiO_2 composite photocatalyst was ultimately obtained through a series of processes, including centrifugation, washing, drying, and calcination at 350 °C and room temperature for 3 h, in which ZnO accounted for 40% of TiO_2.

Preparation of Cu–ZnO/TiO_2 composite materials: the synthesis of the Cu–ZnO/TiO_2 nanocomposite material was achieved using a simple hydrothermal technique, as illustrated in Fig. 1(a). In the aforementioned B solution, Cu^{2+} is incorporated in varying proportions of 2.5%, 5.0%, 7.5%, 10.0%, and 12.5% relative to the mass of zinc while maintaining constant experimental conditions, to synthesize Cu–ZnO/TiO_2 ternary photocatalysts denoted as *y*%Cu–ZnO/TiO_2.

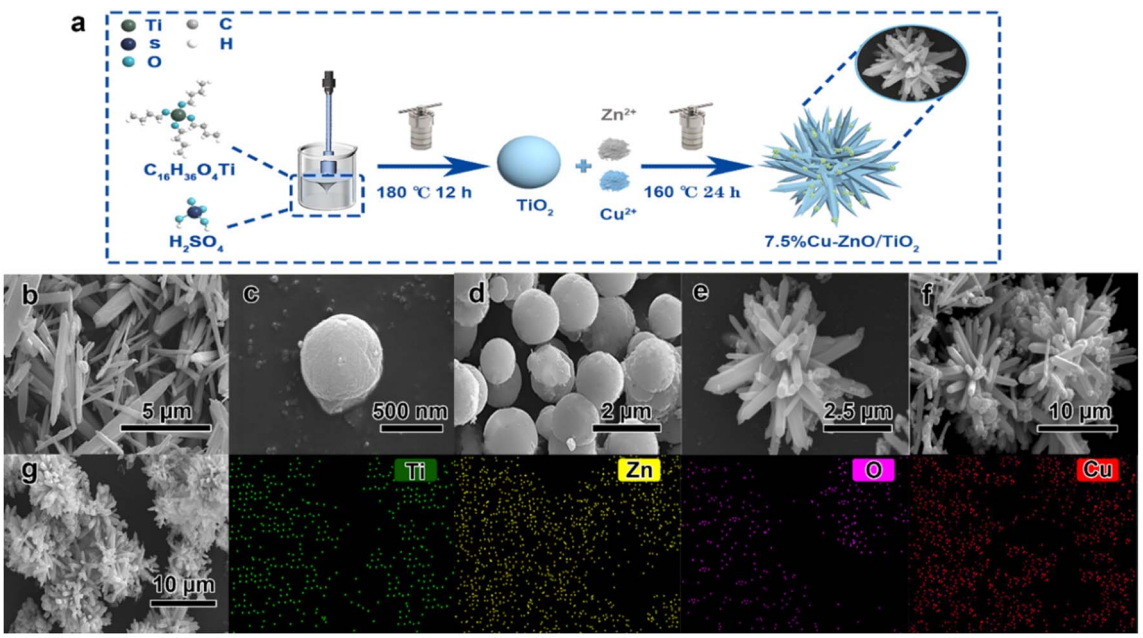

Fig. 1 (a) Schematic diagram of the preparation process for 7.5%Cu–ZnO/TiO_2, (b) ZnO SEM images, (c and d) TiO_2 SEM images, (e and f) SEM images of 7.5%Cu–ZnO/TiO_2 and (g) EDS elemental mapping image of 7.5%Cu–ZnO/TiO_2 showing Ti, Zn, O, and Cu.

2.3 Photodegradation of organic sulfides

The present study utilized an *n*-octane solvent containing dibenzothiophene (DBT) as a representative oil model to assess the photocatalytic degradation activity of sulfur-containing organic compounds. In a typical desulfurization experiment, 0.10 g of photocatalyst was uniformly dispersed within a quartz tube containing 50 ml of simulated oil with a concentration of 10 mg L^{-1}. Firstly, samples were collected after 30 min of stirring under dark conditions to achieve adsorption–desorption equilibrium. Subsequently, the samples were exposed to ultraviolet light and sampled at 30 min intervals throughout the reaction process, with approximately 3 ml of sample collected each time. To ensure accurate data analysis, it is imperative to promptly centrifuge and separate the sample after completing the reaction, and then transfer it into a properly labeled sample vial. A quantitative analysis was conducted on the filtrate using a UV-9000 ultraviolet-visible spectrophotometer to estimate the degradation efficiency. The concentration of DBT in the supernatant is determined by establishing a correlation between absorbance and concentration. The influence of degradation parameters, such as the initial concentration of DBT, catalyst dosage, and catalyst composition ratio on degradation efficiency was investigated and optimized through single-factor experiments. Finally, the degradation efficiency is calculated based on eqn (1):[20]

$$\text{Degradation rate (\%)} = [(C_0 - C_t)/C_0] \times 100 = [(A_0 - A_t)/A_0] \quad (1)$$

In this context, C_0 and C_t represent the initial concentration and real-time concentration (mg L^{-1}) of DBT at time t (min), while A_0 and A_t correspond to the absorbance of DBT at the beginning point and different time intervals (t), respectively. The breakdown of organic pollutants using photocatalysis generally follows a kinetic model that resembles pseudo-first-order kinetics, as indicated by previous research findings. Therefore, this study examined the kinetics characteristics of DBT photocatalytic degradation using the pseudo-first-order kinetic equation.

$$\ln C_t/C_0 = -kt \quad (2)$$

In this equation, k represents the apparent rate constant (min^{-1}); the parameters C_0 and C_t are analogous to those in eqn (1), while t denotes the duration of the reaction (min).

The experiment evaluated the role of active substances in the PODS system by trapping superoxide radicals, hydroxyl radicals, holes and electrons.

3 Results and discussion

3.1 Physical and chemical properties

After conducting SEM analysis (Fig. 1), it was observed that the synthesized microstructure of ZnO consists of nanoneedle, while TiO_2 nanoparticles were uniformly dispersed in a spherical shape with a rough surface, exhibiting a diameter ranging from 400 to 600 nm. In the composite catalyst of 7.5%Cu–ZnO/TiO_2, the TiO_2 nanospheres act as the core and are decorated with needle-like ZnO nanoneedles. EDS spectrum analysis confirmed the successful integration of all components in the ternary photocatalyst.

The XPS spectrum measurement reveals the presence of four elements, namely O, Ti, Zn, and Cu in 7.5%Cu–ZnO/TiO_2 in Fig. 3(a–e). In the case of pure TiO_2, the energy peaks detected at 458.78 eV and 464.48 eV can be ascribed to the orbitals of Ti $2p_{3/2}$ and Ti $2p_{1/2}$, respectively. Moreover, the observed spacing between these peaks measuring 5.70 eV strongly indicates that titanium exists in its +4 oxidation state.[21–23] In the ZnO/TiO_2 and 7.5%Cu–ZnO/TiO_2 samples, the observation of shoulder bands attributed to Ti^{3+} $2p_{1/2}$ and Ti^{3+} $2p_{3/2}$ suggests that oxygen vacancies have been incorporated into the composite photocatalysts.[24,25] Previous studies have demonstrated the crucial role played by the oxidation state of titanium in determining the catalytic efficiency of compounds that incorporate this element. As the reaction progresses, there is an observed augmentation in the Ti^{3+}/Ti^{4+} ratio, leading to an enhancement in the photocatalytic effect of composite catalysts.[26] The Zn 2p spectrum reveals energy bands at 1022.18 eV and 1045.28 eV for Zn $2p_{3/2}$ and Zn $2p_{1/2}$, respectively, exhibiting a binding energy difference of 23.1 eV between the two orbitals. Consequently, it can be inferred that zinc predominantly exists in the form of Zn^{2+} and readily forms stable chemical bonds (Zn–O bonds) with oxygen atoms.[27,28] The measured binding energies of Cu $2p_{3/2}$ and Cu $2p_{1/2}$ are determined to be 931.18 eV and 950.98 eV, respectively, indicating a consistent energy difference of 19.8 eV between the two orbitals. This value corresponds to the standard spin–orbit components associated with Cu 2p.[29] There are two main peaks at 931.28 and 951.28 eV, and further deconvolution reveals four peaks. The peaks at 931.18 eV and 950.98 eV are generated by Cu^0, and the peaks at 932.28 eV and 951.98 eV are generated by Cu^{2+}. In the spectrum of 7.5%Cu–ZnO/TiO_2, three distinct peaks can be observed, representing oxygen species associated with the crystal lattice (O_L), oxygen vacancies (O_V), and adsorbed oxygen molecules (O_{ad}). The 7.5%Cu–ZnO/TiO_2 catalyst in the three comparative samples exhibits a significantly increased presence of oxygen vacancies, which undoubtedly plays a pivotal role in augmenting the catalyst's activity. In summary, this comprehensive XPS analysis provides a meticulous understanding of the elemental composition and chemical intricacies, validating the intricate interplay among doping, defect formation, and enhanced catalytic performance in 7.5%Cu–ZnO/TiO_2 nanomaterials.

The crystal structures of ZnO, TiO_2, ZnO/TiO_2 and 7.5%Cu–ZnO/TiO_2 nanocomposites were studied by XRD. The X-ray diffraction (XRD) patterns of ZnO exhibit a strong similarity to the hexagonal phase of wurtzite, which is represented by JCPDS no. 36-1451. The XRD patterns of TiO_2 closely resemble the anatase structure as indicated by JCPDS no. 21-1272. For 7.5% Cu–ZnO/TiO_2 samples, XRD shows only the characteristic peaks of anatase TiO_2 (101), (103), (200), (105), (211) and (204) and sphalerite hexagonal ZnO high intensity peaks of (100), (002), (101), (102), (110), (103), (200), (112) and (201) crystal faces. The absence of diffraction peaks at 2θ values of 27° and 31° suggests the exclusive presence of the pure anatase phase of TiO_2, indicating no evidence for either rutile or brookite phases.[30] After

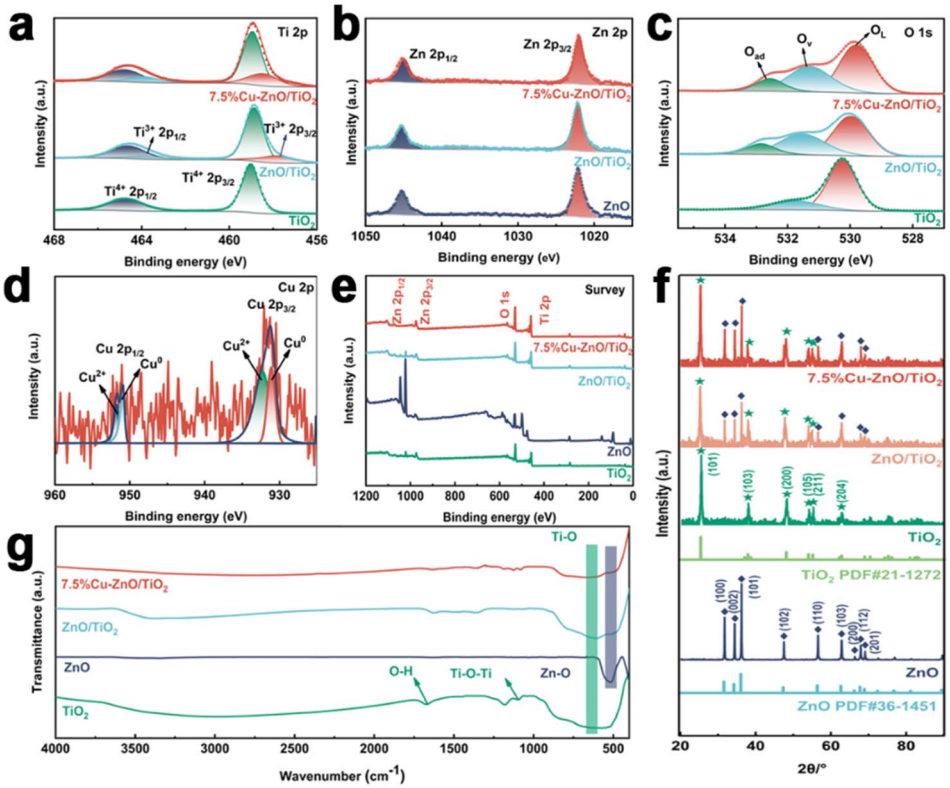

Fig. 2 (a–d) X-ray photoelectron spectroscopy (XPS) spectra with enhanced resolution for Ti 2p, Zn 2p, O 1s, and Cu 2p, (e) XPS full spectrum, (f) XRD pattern, (g) the FT-IR spectrum.

observing the diffraction peak at a 2θ angle of 37.9° for the (004) plane and identifying the appearance of the diffraction peak at a 2θ angle of 48.2° for the (200) crystal plane, it was inferred that there was growth in crystalline structure along the (001) orientation. By XRD analysis, it is obvious that no traces of copper, copper-containing oxides and binary titanium–copper phases are observed in the atlas.[31,32] It may be because the diffraction peaks of TiO_2 and Cu overlap or Cu exists in trace form, which is lower than the detection limit of XRD method.[33,34]

In Fig. 2(g), the absorption peaks observed at 3442 cm^{-1} and 1649 cm^{-1} can be attributed to the vibrational motions of O–H bonds, specifically involving stretching and bending movements, induced by the presence of water adsorbed on the catalyst's surface.[35] The observed peaks in the spectral ranges at 665 cm^{-1} and 1090 cm^{-1} can be attributed to the stretching vibrations of Ti–O bonds and the bending vibrations of the Ti–O–Ti framework, respectively. The stretching vibration of Zn–O bonds is manifested by a peak observed at 499 cm^{-1} in pure ZnO. However, in the composite catalyst of 7.5%Cu–ZnO/TiO_2, this peak undergoes a redshift to 481 cm^{-1}.[36] The spectral curves obtained from FT-IR analysis of ZnO/TiO_2 and 7.5%Cu–ZnO/TiO_2 exhibit remarkable similarities. The absence of a prominent peak at 660 cm^{-1}, associated with the stretching vibration of Cu–O, suggests an extremely low copper concentration that remains undetectable through infrared spectroscopy. The results obtained from XPS analysis are consistent with this finding. The peak shape and position of each catalyst in the figure demonstrate a high degree of consistency, indicating that the modified catalysts effectively retain the original crystal structure of TiO_2. The absence of any spurious peaks following modification suggests that the composite material possesses a well-defined crystalline structure without any impurities, which aligns with the XRD findings.

The absorption characteristics of TiO_2, ZnO, ZnO/TiO_2, and 7.5%Cu–ZnO/TiO_2 were observed to be particularly strong in the wavelength range of 200–400 nm as shown in Fig. 3(a). This observation suggests that the prepared photocatalyst primarily exhibits adsorption capacity in the ultraviolet region. The light response intensity in the ultraviolet region of the 7.5%Cu–ZnO/TiO_2 composite material demonstrates a comparatively reduced intensity when compared to that observed for pure TiO_2. Moreover, there is a noticeable shift in the light response range from 389 nm to approximately 459 nm, indicating that the integration of TiO_2 and ZnO through a heterojunction significantly enhances the efficiency of light energy utilization. The central peak position of four-coordinated titanium is observed at 220 nm, while the central peak position of six-coordinated titanium falls within the range of 240 nm and 300 nm.[37,38] The graph indicates that Ti primarily exists in a six-coordinated state within the composite photocatalyst. In order to calculate the band gap width of photocatalyst, the Kubelka–Munk formula is used:[39,40]

$$(\alpha h\nu)^{1/2} = A(h\nu - E_g) \quad (3)$$

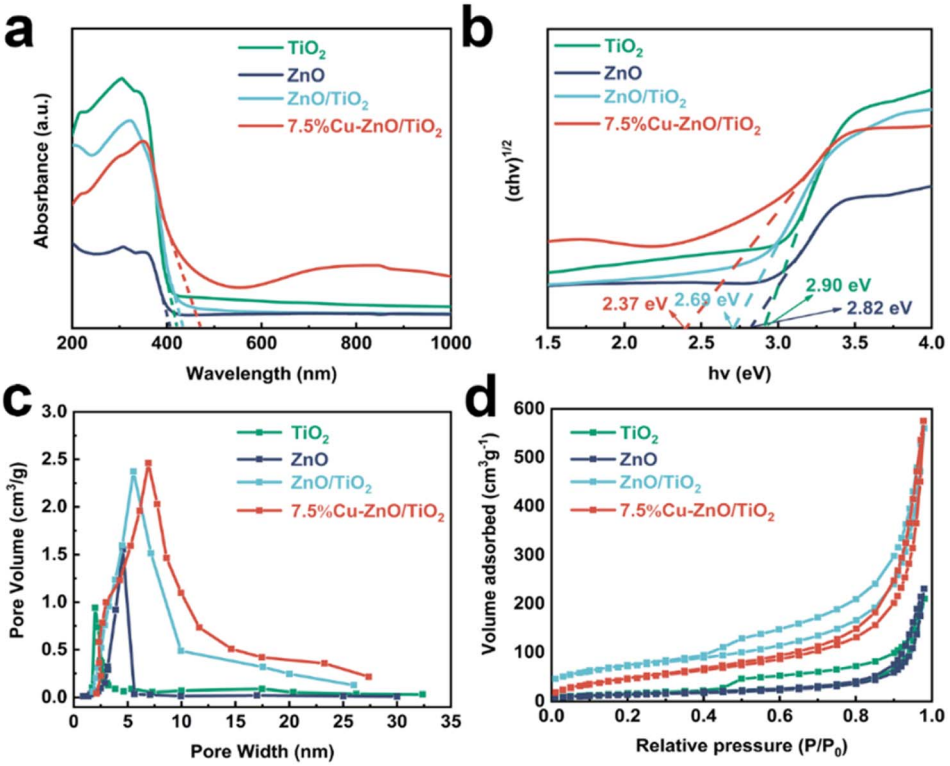

Fig. 3 (a) Ultraviolet-visible diffuse reflectance spectroscopy, (b) optical bandgap energy, (c) N_2 adsorption–desorption isotherm curve, (d) pore size distribution graph.

In the formula, A, α, h, ν and E_g are respectively proportionality constant, absorption coefficient, Planck constant, incident light frequency and band gap width. As can be seen from Fig. 3(b), the bandgap widths of TiO_2, ZnO, ZnO/TiO_2 and 7.5%Cu–ZnO/TiO_2 are 2.90 eV, 2.82 eV, 2.69 eV and 2.37 eV, respectively. The composite catalyst exhibits the presence of heterojunctions, which leads to a narrower bandgap width in 7.5%Cu–ZnO/TiO_2. This promotes the movement of electrons across energy barriers, stimulates the generation of hole–electron pairs, enhances light absorption and utilization, thereby improving the photocatalytic desulfurization performance of the sample. The confirmation of the hypothesis was achieved by conducting experiments that utilized a pair of catalysts for ultraviolet light-induced photocatalytic desulfurization.

As shown in Fig. 3(c), the photocatalysts TiO_2, ZnO, ZnO/TiO_2, and 7.5%Cu–ZnO/TiO_2 exhibited type IV isotherms with H3 hysteresis loops, indicating the presence of mesopores on their surfaces.[41] The pore distribution depicted in Fig. 3(d) further confirms this point and indicates a relatively even distribution. The homogeneity of this structure suggests an increased availability of catalytic sites, diffusion pathways, and overall surface reactivity. The calculated results for the specific surface area and pore parameters of the prepared photocatalysts are presented in summarized Table 1.† The BET surface areas of TiO_2, ZnO, ZnO/TiO_2, and 7.5%Cu–ZnO/TiO_2 are recorded as 38.21 $m^2\ g^{-1}$, 40.15 $m^2\ g^{-1}$, 73.612 $m^2\ g^{-1}$, and 80.159 $m^2\ g^{-1}$, in Table 1, respectively. It is evident that the specific surface area of 7.5%Cu–ZnO/TiO_2 exceeds that of TiO_2, ZnO, and ZnO/TiO_2, suggesting an enhancement in the specific surface area resulting from the incorporation of a ternary catalyst composite. This leads to an increased quantity of active sites present on the surface, resulting in enhanced adsorption of compounds containing sulfur and thus improving the photocatalytic performance. Furthermore, the observed increase in specific surface area and pore size indirectly indicates an enhanced interface contact between Cu, ZnO, and TiO_2.

3.2 Photocatalytic performance

In this research, we conducted an analysis on the physicochemical characteristics of a newly developed photocatalyst. Additionally, we evaluated its efficacy in degrading a persistent DBT-simulated pollutant under UV-visible light exposure for a duration of 210 minutes. The original ZnO and TiO_2, as depicted in Fig. 4(a), exhibited removal rates of 25.48% and 42.96% for DBT, indicating their relatively low photocatalytic

Table 1 The structural characteristics of TiO_2, ZnO, ZnO/TiO_2, and 7.5%Cu–ZnO/TiO_2

Catalyst	BET surface area ($m^2\ g^{-1}$)	Average pore size (nm)	Pore volume ($m^2\ g^{-1}$)
TiO_2	38.21	3.055	0.047
ZnO	40.15	22.74	0.086
ZnO/TiO_2	73.612	17.357	0.218
7.5%Cu–ZnO/TiO_2	80.159	24.226	0.201

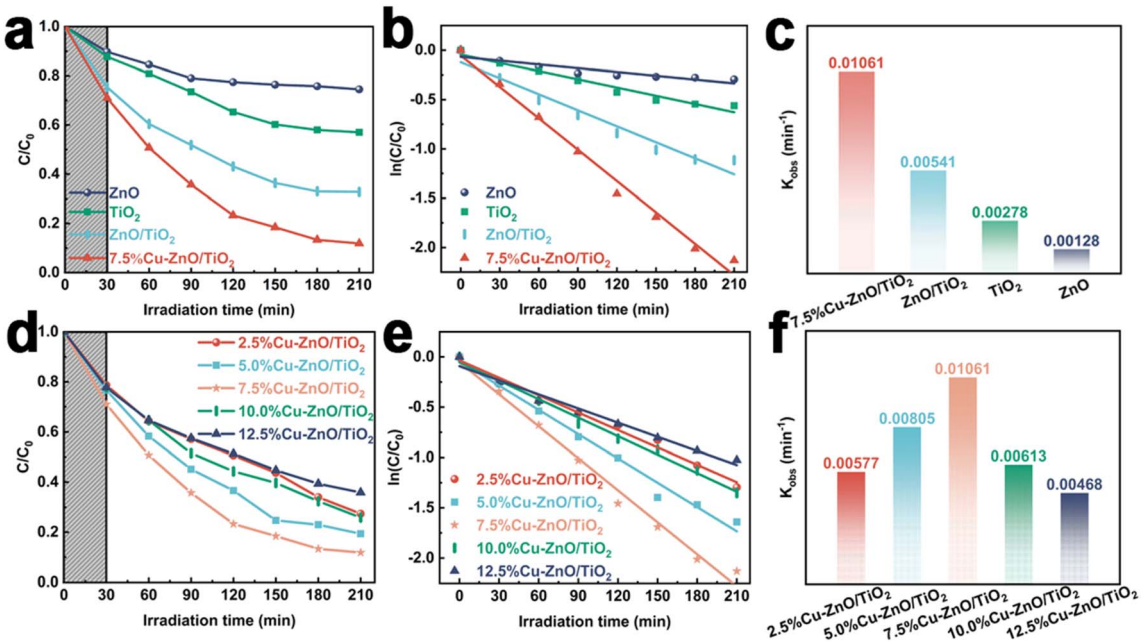

Fig. 4 (a) Degradation curves of DBT were studied under photolytic conditions using TiO_2, ZnO, ZnO/TiO_2 and 7.5%Cu–ZnO/TiO_2, (d) optimizing the copper loading quantity to maximize the efficiency of Cu–ZnO/TiO_2 in photocatalytic degradation, (b and e) corresponding first-order dynamic curve, (c and f) frequency distribution of k values depicted in figure d and e, (reaction conditions: photocatalyst dosage 10 mg, DBT concentration 50 mg L^{-1}).

activity. However, the binary composite system of ZnO/TiO_2 demonstrated a significantly enhanced photocatalytic degradation rate of 67.24%, surpassing that of pure ZnO and TiO_2. The degradation rate of 7.5%Cu–ZnO/TiO_2 is the highest, reaching approximately 88.12%. The main explanation for the high rate of photocatalytic degradation in Cu–ZnO/TiO_2 is as follows:[42–44] (a) the construction of Z-type heterojunctions facilitates the efficient separation and transport of photogenerated electrons and holes. (b) Copper, being an effective conductor for the transportation of electrons and holes, exhibits the capability to promote the separation and transfer of electron–hole pairs produced by light, thereby augmenting light absorption. (c) The presence of oxygen defects provides numerous sites for photocatalytic reactions during the process. (d) Compared to binary ZnO/TiO_2 photocatalysts and monolithic ZnO or TiO_2, ternary nanocomposites demonstrate an increased surface area. The experimental section presents a detailed analysis of the photodegradation process of DBT, employing the pseudo-first-order kinetic model for assessment. It is evident that there exists a significant linear relationship between the natural logarithm of (C_t/C_0) and the reaction duration (t), indicating adherence to a pseudo-first-order kinetic equation (Fig. 4(b)). Fig. 4(c) presents a histogram that illustrates the values of the apparent rate constant (k) derived from Fig. 4(b). Significantly, the 7.5%Cu–ZnO/TiO_2 exhibits a remarkable DBT removal efficiency of 0.01061 min^{-1}, surpassing ZnO by a factor of 8.23 (0.00128 min^{-1}), TiO_2 by a factor of 3.82 (0.00278 min^{-1}), and ZnO/TiO_2 by a factor of 1.96 (0.00541 min^{-1}). The research mentioned above suggests that the combined utilization of Cu, ZnO, and TiO_2 can greatly improve the effectiveness of photocatalytic oxidation in desulfurization. Additionally, as the percentage of Cu mass in Cu–ZnO/TiO_2 increases, there is a distinct trend of initial enhancement followed by a decline in the photocatalytic degradation rate of DBT (Fig. 4(d)). This occurrence can be ascribed to the effective transmission of interface charges and the extended duration of electron–hole transfer, which effectively enhance the photocatalytic efficacy of the catalyst under optimal Cu loading conditions. However, an excessive amount of copper loading leads to a decline in photo performance as it hampers the efficient generation of electron–hole pairs and promotes an increased recombination rate. It is noteworthy that the degradation rate of the photocatalyst (7.5%Cu–ZnO/TiO_2), which was formed with a mass fraction of 7.5%Cu in Cu–ZnO/TiO_2 reached 88.12%. In comparison, the photocatalytic degradation rates of Cu–ZnO/TiO_2 with different concentrations (2.5%, 5.0%, 10.0%, and 12.5%) were measured as follows: 72.62%, 80.62%, 74.12%, and 64.12%, respectively (Fig. 4(d)). In addition, the photocatalytic reactions demonstrate a kinetic process that exhibits pseudo-first-order behavior (Fig. 4(e)). The rate constants (K values) for these reactions are as follows: 0.00577 min^{-1} (2.5%Cu–ZnO/TiO_2), 0.00805 min^{-1} (5.0%Cu–ZnO/TiO_2), 0.01061 min^{-1} (7.5%Cu–ZnO/TiO_2), 0.00613 min^{-1} (10.0%Cu–ZnO/TiO_2), and 0.00468 min^{-1} (12.5%Cu–ZnO/TiO_2). Consequently, the optimal photocatalyst is determined to be the one with a composition of 7.5%Cu–ZnO/TiO_2.

Factors such as catalyst dosage, sulfide concentration, and types of sulfides were studied to investigate and optimize the conditions for enhancing the efficiency of DBT removal through photocatalysis. The optimal catalyst dosage for achieving the

highest photocatalytic degradation efficiency is found to be 10 mg, exhibiting an impressive rate of 88.12% as depicted in Fig. 5(a). However, in cases where the catalyst concentration falls below a certain threshold, augmenting the quantity of photocatalyst can enhance both the effective specific surface area and the quantity of active sites. As a result, there is an enhanced production of hydroxyl groups and superoxide radicals, leading to a substantial enhancement in photocatalytic performance. The opacity of the suspension increases further when the dosage of photocatalyst exceeds 10 mg due to the effects of light shielding and scattering, resulting in a decrease in degradation efficiency. The corresponding k values for different concentrations of DBT are 0.00439 min^{-1} (5 mg), 0.01061 min^{-1} (10 mg), 0.00806 min^{-1} (15 mg), 0.00565 min^{-1} (20 mg), and 0.00438 min^{-1} (25 mg) respectively, as shown in Fig. 5(b). As depicted in Fig. 5(d), within the 7.5%Cu–ZnO/TiO_2 system, an increase in DBT concentration from 10 mg L^{-1} to 200 mg L^{-1} results in a decrease in its degradation rate from 88.12% to 44.87%, highlighting the significant impact of initial DBT concentration on pollutant removal efficiency. There are two primary factors that contribute to this phenomenon:[45,46] (a) the elevation of DBT concentration in the water leads to a reduction in light transmittance, thereby diminishing the number of effective photons. (b) During the degradation process of high-concentration DBT solutions, a substantial quantity of intermediates is generated, which compete with DBT compete with DBT compounds for the process of adsorption and photodegradation. Meanwhile, the aforementioned photodegradation process also follows a pseudo-first-order kinetic model (Fig. 5(e)), with corresponding rate constants (Fig. 5(f)) of 0.01219 min^{-1} (10 mg L^{-1}), 0.01061 min^{-1} (50 mg L^{-1}), 0.00567 min^{-1} (100 mg L^{-1}), 0.00445 min^{-1} (150 mg L^{-1}), and 0.00253 min^{-1} (200 mg L^{-1}). Significant variations in the degradation efficiency of 50 mg DBT, BT (benzothiophene), and T (thiophene) were observed after degradation using a 10 mg 7.5%Cu–ZnO/TiO_2 photocatalyst. The photocatalyst demonstrates distinct variations in removal efficiency for three different sulfur-containing compounds, as depicted in Fig. 5(g). It achieves the highest degradation efficiency of 88.12% for DBT, while BT and T demonstrate degradation efficiencies of 77.38% and 74.78%, respectively. The degradation of three distinct compounds containing sulfur also follows a kinetic model that can be approximated as pseudo-first-order (Fig. 5(h)). The corresponding rate constants for DBT, BT, and T are measured to be 0.01061 min^{-1}, 0.00707 min^{-1}, and 0.00599 min^{-1} respectively (Fig. 5(i)).

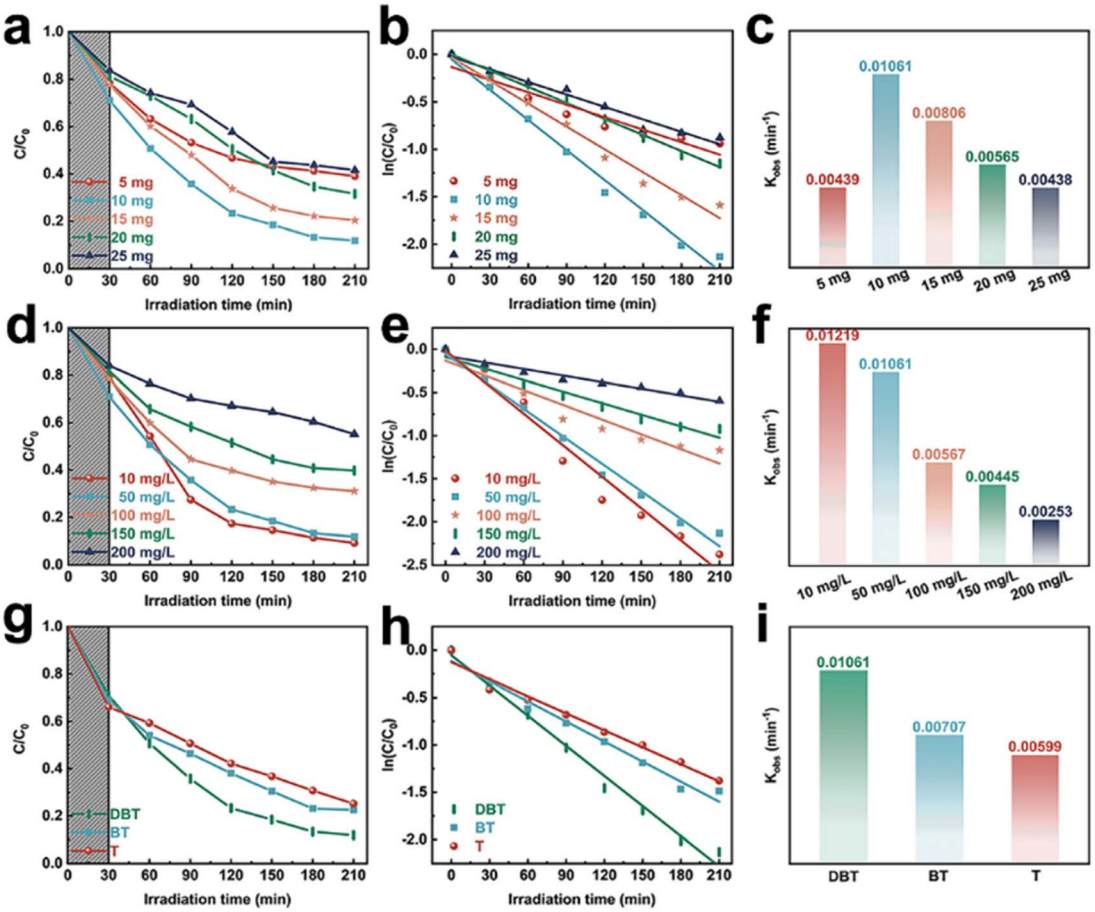

Fig. 5 (a) Catalyst dosage, (d) initial concentration of DBT, (g) type of sulfide species, (b, e and h) corresponds to the first-order dynamic curve, (c, f and i) histograms of k values obtained from figures b, e and h.

After conducting 5 consecutive photocatalytic experiments for DBT removal, the reusability and stability of 7.5%Cu–ZnO/TiO_2 were assessed under identical conditions, which are crucial factors to consider in practical applications. After 5 cycles, as depicted in Fig. 6(a), the degradation rate of the 7.5% Cu–ZnO/TiO_2 photocatalyst remains at 80.69%, indicating its inherent stability. The degradation rate has exhibited a slight decrease, potentially attributed to losses incurred during the process of photocatalyst recovery. Furthermore, the XRD, FT-IR, and SEM results (Fig. 6(b–d)) demonstrate that there were no noticeable changes in the crystallographic planes, characteristic peaks or morphology after five cycles of testing. This provides additional validation for the exceptional stability and reproducibility of 7.5%Cu–ZnO/TiO_2. After conducting further evaluation of the stability of 7.5%Cu–ZnO/TiO_2 using XPS, a comprehensive energy spectrum analysis was performed for each individual element. The elemental composition of 7.5% Cu–ZnO/TiO_2 remained unchanged during the photocatalytic reaction. No noticeable alterations were detected in the Ti 2p and Zn 2p spectra, as well as in the XPS full spectrum before and after the light reaction (see Fig. 6(e–h)). In the O 1s spectrum, both the concentration of oxygen vacancies (Ov) and the total oxygen content exhibited significant increases, which can be attributed to the adsorption of oxygen on the surface of 7.5% Cu–ZnO/TiO_2 after testing.[47] The comprehensive characterization conducted after testing confirmed minimal changes in the 7.5%Cu–ZnO/TiO_2 photocatalyst before and after light reaction, providing compelling evidence of its exceptional stability and reproducibility.

3.3 Possible photocatalytic mechanisms

Based on the analysis of the physical and chemical properties of TiO_2, ZnO, ZnO/TiO_2, and specifically 7.5%Cu–ZnO/TiO_2, a potential mechanism for DBT photodegradation by 7.5%Cu–ZnO/TiO_2 was proposed. The photocatalytic performance of the composite material can be significantly improved due to the effective suppression of electron–hole recombination, which is achieved by promoting efficient charge transfer among individual semiconductors in the 7.5%Cu–ZnO/TiO_2 nanocomposite material. Hence, acquiring a comprehensive comprehension of the band edges of individual materials within the 7.5%Cu–ZnO/TiO_2 system holds immense importance in accurately grasping its underlying mechanism. The formula is used to calculate the conduction band (CB) and valence band (VB) of TiO_2 and ZnO:[48–50]

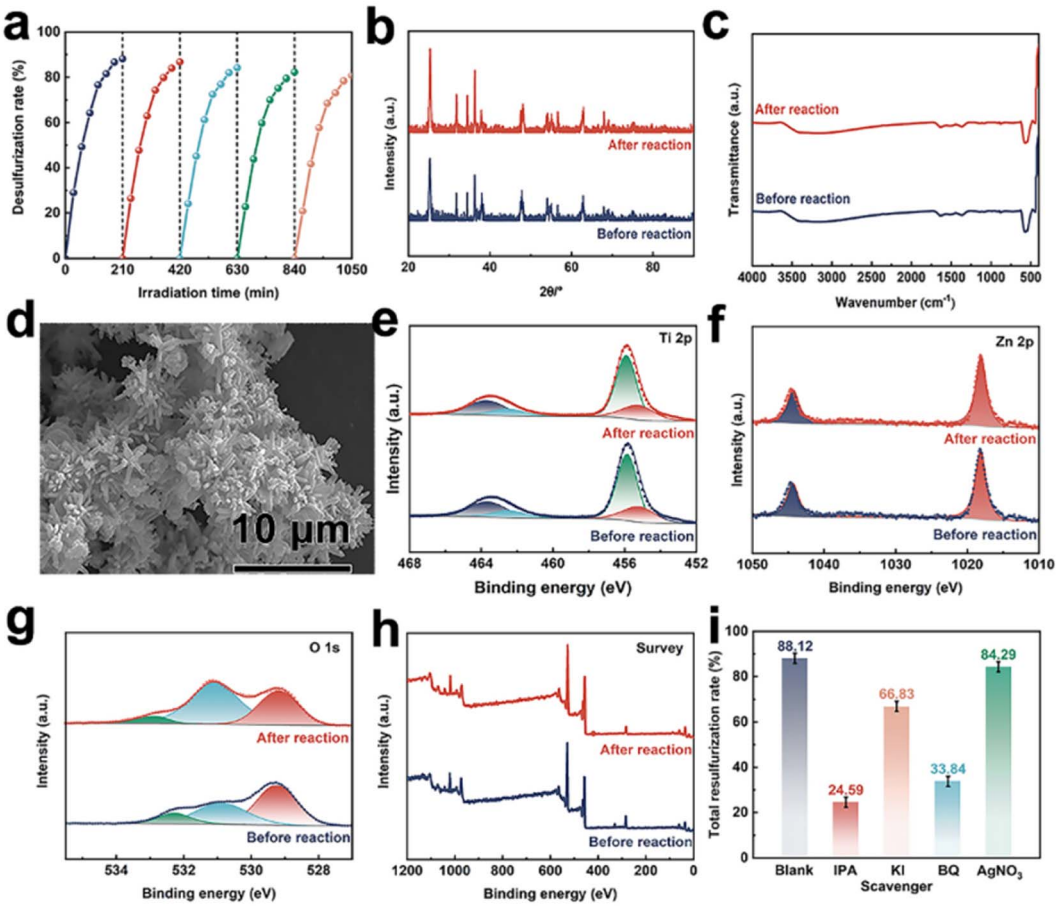

Fig. 6 Recycling experiment, free radical scavenging experiment, and characterization after photocatalysis of 7.5%Cu–ZnO/TiO_2 catalyst (a) recycling experiment, (b) XRD spectrum, (c) FT-IR spectrum, (d) SEM image, (e–g) XPS energy spectra of Ti 2p, Zn 2p, and O 1s, (h) XPS full spectrum, (i) free radical scavenging experiment.

$$E_{CB} = X - E^{C} - 0.5E_{g} \quad (4)$$

$$E_{VB} = X - E^{C} + 0.5E_{g} \quad (5)$$

In the given equation, the CB and VB edge potentials are denoted by E_{CB} and E_{VB} respectively. X represents electronegativity, with ZnO having an electronegativity of 5.94 eV and TiO_2 having an electronegativity of 5.89 eV; the band gap energy is denoted as E_g, with values of 2.82 eV for ZnO and 2.90 eV for TiO_2; E^C denotes the energy of free electrons relative to hydrogen (4.5 eV). After performing the necessary calculations, it was determined that ZnO exhibits a CB potential of 0.03 eV and a VB potential of 2.85 eV, while TiO_2 displays a CB potential of −0.06 eV and a VB potential of 2.84 eV.

To investigate the function of 7.5%Cu–ZnO/TiO_2 in the PODS system, experiments were conducted to determine the active components and evaluate their capability for free radical elimination. Different substances, including isopropyl alcohol (IPA), potassium iodide (KI), benzoquinone (BQ), and silver nitrate ($AgNO_3$), were utilized as scavengers to capture hydroxyl radicals ($^{\bullet}OH$), holes (h^+), superoxide radicals ($^{\bullet}O^{2-}$), and electrons (e^-).[51,52] The specific experimental procedure was consistent with that of the photocatalytic desulfurization process. The desulfurization rate exhibits a descending trend, as shown in Fig. 6(i), with the following order of decrease: blank sample, $AgNO_3$, KI, BQ, and IPA. In the absence of any scavengers, the desulfurization efficiency of 7.5%Cu–ZnO/TiO_2 reaches 88.12% after 210 min. However, the addition of KI and $AgNO_3$ to the target sulfide does not significantly affect the degradation of DBT by 7.5%Cu–ZnO/TiO_2, indicating that neither h^+ nor e^- are active species in this system. In contrast, the addition of IPA and BQ significantly reduces the desulfurization efficiency of 7.5% Cu–ZnO/TiO_2 towards DBT, with reductions of 63.53% and 54.28%, respectively. This emphasizes the significant contributions of both ·OH and $^{\bullet}O^{2-}$ in the elimination mechanism of DBT by 7.5%Cu–ZnO/TiO_2, with $^{\bullet}OH$ demonstrating superior efficacy compared to $^{\bullet}O^{2-}$.

Based on the experimental findings and relevant literature, Fig. 7 depicts the photocatalytic mechanism exhibited by 7.5% Cu–ZnO/TiO_2.[15,53–55] In general, ZnO/TiO_2 exhibits a type II heterojunction between TiO_2 and ZnO, which facilitates the efficient degradation of DBT. In the II-type ZnO/TiO_2 heterojunction, TiO_2 predominantly captures electrons while ZnO accumulates holes, effectively inhibiting charge carrier recombination and thus enhancing photocatalytic performance. However, the research focus has shifted towards Z-type heterojunctions due to the Coulomb repulsion effect among photogenerated electrons. The electron migration effect is enhanced in a Z-type heterojunction, which promotes efficient charge transfer between semiconductor interfaces. In the proposed nano-composite photocatalyst, Cu facilitates electron migration between ZnO and TiO_2, thereby accelerating interfacial electron transfer in the 7.5%Cu–ZnO/TiO_2 composite catalyst and significantly enhancing its photocatalytic activity.

First, the sulfide in the oil phase is adsorbed on the surface of the adsorption site of the composite catalyst under the action of polarity. Subsequently, the oxidation reaction of the sulfide occurs at the catalytic site of the composite catalyst, that is, under the irradiation of ultraviolet light, e^- excites from the valence band to the conduction band, resulting in photogenerated electron–hole pairs. e^- reacts with molecular oxygen to form $^{\bullet}O^{2-}$, which further reacts with H_2O or OH^- to form $^{\bullet}OH$ radical. At the same time, h^+ reacts with dissolved water to produce highly oxidizing $^{\bullet}OH$. Hydroxyl radical ($^{\bullet}OH$) and superoxide radical ($^{\bullet}O^{2-}$) were responsible for the degradation

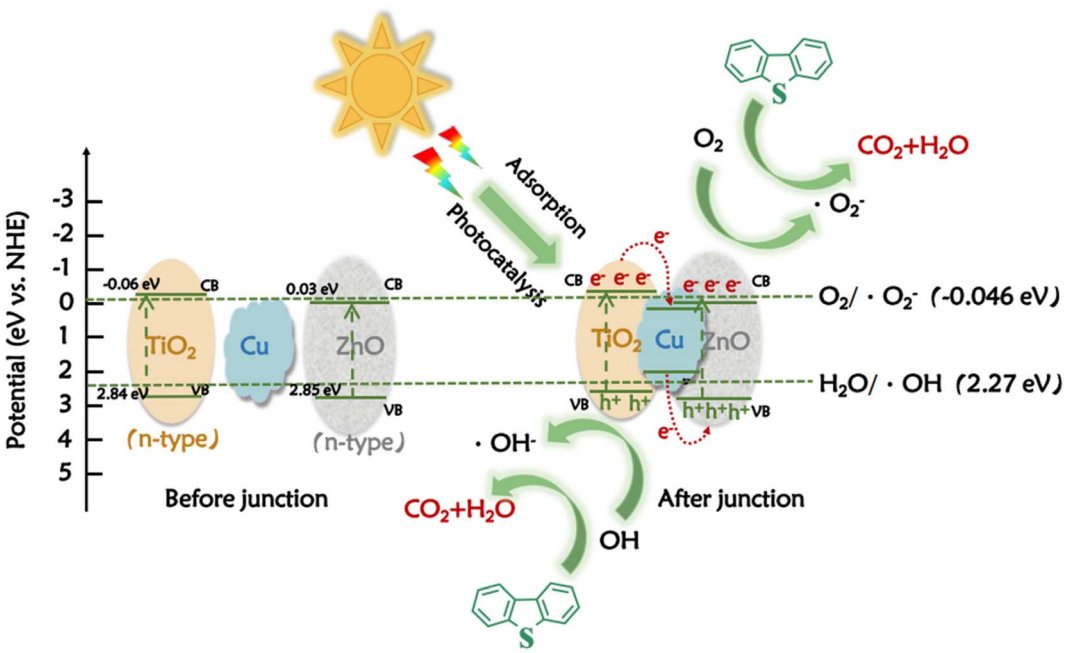

Fig. 7 The potential mechanism underlying the photocatalytic decomposition of DBT using 7.5%Cu–ZnO/TiO_2 is being studied.

of DBT. In addition, in the 7.5%Cu–ZnO/TiO_2 composite photocatalyst, the Fermi level of Cu exhibits a higher position compared to the conduction band (CB) level of TiO_2, thereby facilitating effective electron transfer from the CB level of TiO_2 to Cu. At the same time, there is a difference in the Fermi level between Cu and the VB level of ZnO, which facilitates the movement of electrons from accumulated Cu to the VB level of ZnO. This procedure effectively suppresses the presence of photo-induced vacancies in ZnO and enhances the efficiency of segregating photo-generated electrons in ZnO, resulting in a significant improvement in its reduction potential. Therefore, the 7.5%Cu–ZnO/TiO_2 nanocomposite photocatalyst exhibits excellent photocatalytic activity and can effectively promote the degradation of DBT.

4 Conclusion

In this paper, Z-type heterostructures with a large number of defects were successfully constructed using a simple hydrothermal synthesis method and applied to DBT photocatalysts that are difficult to degrade. By adjusting the mass percentage of Cu and the operating parameters of Cu–ZnO/TiO_2 photocatalyst, the best photocatalytic activity was achieved, resulting in a removal rate of DBT as high as 88.12%. The 7.5%Cu–ZnO/TiO_2 catalyst exhibited good repeatability and stability, and the improvement in photocatalytic performance can be attributed to the construction of Z-type heterojunctions and the utilization of Cu as a charge transport channel. This provides a new approach for degrading DBT using titanium-based photocatalytic materials.

Data availability

The authors confirm that the data supporting the findings of this study are available within the article.

Conflicts of interest

The authors declare that they are aware of any competing financial interests or personal relationships that could have appeared to influence the work reported in this paper. This manuscript is submitted without any conflicts of interest and has been published with the consent of all authors. On behalf of my co-authors, I would like to state that the work described is original research that has not been previously published and is not being considered for publication elsewhere, either in whole or in part. The listed authors have agreed to the attached manuscript.

Acknowledgements

The authors are grateful for the Project supported by the National Natural Science Foundation of China (Grant no. 52172092).

References

1 X. Zhou, T. Wang, H. Liu, X. Gao, C. Wang and G. Wang, Desulfurization through photocatalytic oxidation: a critical review, *ChemSusChem*, 2021, **14**(2), 492–511.
2 K. Chen, X.-M. Zhang, X.-F. Yang, M.-G. Jiao, Z. Zhou, M.-H. Zhang, D.-H. Wang and X.-H. Bu, Electronic structure of heterojunction MoO_2/g-C_3N_4 catalyst for oxidative desulfurization, *Appl. Catal., B*, 2018, **238**, 263–273.
3 R. Wang, X. Xie, C. Xu, Y. Lin, D. You, J. Chen, Z. Li, Z. Shi, Q. Cui and M. Wang, Bi-piezoelectric effect assisted ZnO nanorods/PVDF-HFP spongy photocatalyst for enhanced performance on degrading organic pollutant, *Chem. Eng. J.*, 2022, **439**, 135787.
4 M. Li, P. Li, L. Zhang, M. Chen, J. Tang, C. Qin, S. L. J. Lee and S. Lin, Facile fabrication of ZnO decorated ZnFe-layered double hydroxides@biochar nanocomposites for synergistic photodegradation of tetracycline under visible light, *Chem. Eng. J.*, 2022, **434**, 134772.
5 S. Y. Sawant, M. S. Sayed, T. H. Han, M. R. Karim, J.-J. Shim and M. H. Cho, Bio-synthesis of finely distributed Ag nanoparticle-decorated TiO_2 nanorods for sunlight-induced photoelectrochemical water splitting, *J. Ind. Eng. Chem.*, 2019, **69**, 48–56.
6 S. G. Kumar and R. Kavitha, Lanthanide ions doped ZnO based photocatalysts, *Sep. Purif. Technol.*, 2021, **274**, 118853.
7 Y. Wan, J. Li, J. Ni, C. Wang, C. Ni and H. Chen, Crystal-facet and microstructure engineering in ZnO for photocatalytic NO oxidation, *J. Hazard. Mater.*, 2022, **435**, 129073.
8 P. Bharathi, S. Harish, J. Archana, M. Navaneethan, S. Ponnusamy, C. Muthamizhchelvan, M. Shimomura and Y. Hayakawa, Enhanced charge transfer and separation of hierarchical CuO/ZnO composites: the synergistic effect of photocatalysis for the mineralization of organic pollutant in water, *Appl. Surf. Sci.*, 2019, **484**, 884–891.
9 Y. Poo-arporn, S. Kityakarn, A. Niltharach, M. F. Smith, S. Seraphin, M. Wörner and A. Worayingyong, Photocatalytic oxidation of thiophene over cerium doped TiO_2 thin film, *Mater. Sci. Semicond. Process.*, 2019, **93**, 21–27.
10 X. Li, Y. Mao, K. Leng, G. Ye, Y. Sun and W. Xu, Enhancement of oxidative desulfurization performance over amorphous titania by doping MIL-101 (Cr), *Microporous Mesoporous Mater.*, 2017, **254**, 114–120.
11 R. Daghrir, P. Drogui and D. Robert, Modified TiO_2 for environmental photocatalytic applications: a review, *Ind. Eng. Chem. Res.*, 2013, **52**(10), 3581–3599.
12 F. Kayaci, S. Vempati, C. Ozgit-Akgun, I. Donmez, N. Biyikli and T. Uyar, Selective isolation of the electron or hole in photocatalysis: ZnO–TiO_2 and TiO_2–ZnO core–shell structured heterojunction nanofibers *via* electrospinning and atomic layer deposition, *Nanoscale*, 2014, **6**(11), 5735–5745.
13 T. D. N. Thi, L. H. Nguyen, X. H. Nguyen, H. V. Phung, T. H. T. Vinh, P. Van Viet, N. Van Thai, H. N. Le, D. T. Pham and H. T. Van, Enhanced heterogeneous photocatalytic perozone degradation of amoxicillin by ZnO

modified TiO_2 nanocomposites under visible light irradiation, *Mater. Sci. Semicond. Process.*, 2022, **142**, 106456.
14 E. Vasilaki, N. Katsarakis, S. Dokianakis and M. Vamvakaki, rGO functionalized ZnO–TiO_2 core–shell flower-like architectures for visible light photocatalysis, *Catalysts*, 2021, **11**(3), 332.
15 V. Lachom, P. Poolcharuansin and P. Laokul, Preparation, characterizations and photocatalytic activity of a ZnO/TiO_2 nanocomposite, *Mater. Res. Express*, 2017, **4**(3), 035006.
16 C. Cheng, A. Amini, C. Zhu, Z. Xu, H. Song and N. Wang, Enhanced photocatalytic performance of TiO_2–ZnO hybrid nanostructures, *Sci. Rep.*, 2014, **4**(1), 4181.
17 J. Song, G. Sun, J. Yu, Y. Si and B. Ding, Construction of ternary Ag@ ZnO/TiO_2 fibrous membranes with hierarchical nanostructures and mechanical flexibility for water purification, *Ceram. Int.*, 2020, **46**(1), 468–475.
18 H. G. Yang, C. H. Sun, S. Z. Qiao, J. Zou, G. Liu, S. C. Smith, H. M. Cheng and G. Q. Lu, Anatase TiO_2 single crystals with a large percentage of reactive facets, *Nature*, 2008, **453**(7195), 638–641.
19 Z. Zhao, Z. Sun, H. Zhao, M. Zheng, P. Du, J. Zhao and H. Fan, Phase control of hierarchically structured mesoporous anatase TiO_2 microspheres covered with {001} facets, *J. Mater. Chem.*, 2012, **22**(41), 21965–21971.
20 S. U. Hassan, H. Khalid, S. Shafique, M. A. Farid, M. H. Saeed, Z. Ali, M. S. Nazir, M. Hussain and Y.-K. Park, Investigating catalytic oxidative desulfurization of model fuel using hollow PW12/TiO_2@$MgCO_3$ and performance optimization *via* Box–Behnken design, *Chemosphere*, 2023, **339**, 139662.
21 X. Chen, J. Zheng, L. Li and W. Chu, Strategy for enhanced performance of silicon nanoparticle anodes for lithium-ion batteries, *RSC Adv.*, 2022, **12**(28), 17889–17897.
22 Y. Li, F. Zhang, K. Xu, Z. Yang and Z. Dong, The synergistic enhancement of photocatalytic activity by Fe_3O_4–TiO_2 nanosheets for rhodamine B degradation, *Colloids Surf., A*, 2024, **700**, 134803.
23 Z. Li, Y. Chu, T. Mi, J. Zhao and F. Meng, Enhanced photocatalytic H_2 evolution over conjugated polymer/Au@TiO_2 ternary heterojunction under visible light: Enriched photons input from polymers, *Colloids Surf., A*, 2024, **692**, 133991.
24 M. Xu, S. He, H. Chen, G. Cui, L. Zheng, B. Wang and M. Wei, TiO_{2-x}-modified Ni nanocatalyst with tunable metal–support interaction for water–gas shift reaction, *ACS Catal.*, 2017, **7**(11), 7600–7609.
25 J. Ji, Two-Stage Ultraviolet Degradation of Perovskite Solar Cells Induced by the Oxygen Vacancy-Ti^{4+} States, *iScience*, 2020, **23**(4), 101013.
26 R. Nawaz, C. F. Kait, H. Y. Chia, M. H. Isa, L. W. Huei, N. T. Sahrin and N. Khan, Manipulation of the Ti^{3+}/Ti^{4+} ratio in colored titanium dioxide and its role in photocatalytic degradation of environmental pollutants, *Surf. Interfaces*, 2022, **32**, 102146.
27 G. Dong, W. Chi, D.-f. Chai, Z. Zhang, J. Li, M. Zhao, W. Zhang, J. Lv and S. Chen, A novel Ag_3BiO_3/ZnO/BC composite with abundant defects and utilizing hemp BC as charge transfer mediator for photocatalytic degradation of levofloxacin, *Appl. Surf. Sci.*, 2023, **619**, 156732.
28 Z. Guo, H. Hou, J. Zhang, P. Cai and J. Lin, Prominent roles of Ni $(OH)_2$ deposited on $ZnIn_2S_4$ microspheres in efficient charge separation and photocatalytic H_2 evolution, *RSC Adv.*, 2021, **11**(20), 12442–12448.
29 C. K. Swamy, A. Hezam, A. M. Ramesh, D. H. Ramakrishnegowda, D. K. Purushothama, J. Krishnegowda and S. Shivanna, Microwave hydrothermal synthesis of copper induced ZnO/gC_3N_4 heterostructure with efficient photocatalytic degradation through S-scheme mechanism, *J. Photochem. Photobiol., A*, 2021, **418**, 113394.
30 L. Gu, J. Wang, H. Cheng, Y. Du and X. Han, Synthesis of nano-sized anatase TiO_2 with reactive {001} facets using lamellar protonated titanate as precursor, *Chem. Commun.*, 2012, **48**(55), 6978–6980.
31 W. Q. Fang, J. Z. Zhou, J. Liu, Z. G. Chen, C. Yang, C. H. Sun, G. R. Qian, J. Zou, S. Z. Qiao and H. G. Yang, Hierarchical structures of single-crystalline anatase TiO_2 nanosheets dominated by {001} Facets, *Chem.–Eur. J.*, 2011, **17**(5), 1423.
32 Y. Pang, G. Xu, Q. Feng, J. Lv, Y. Qin, Y. Zhang, Z. Zheng and Y. Wu, Crystalline orientation preference for TiO_2 nanotube arrays with efficient photoelectrochemical properties, *Phys. Lett. A*, 2018, **382**(38), 2759–2762.
33 B. Xu, L. Dong and Y. Chen, Influence of CuO loading on dispersion and reduction behavior of CuO/TiO_2 (anatase) system, *J. Chem. Soc., Faraday Trans.*, 1998, **94**(13), 1905–1909.
34 A. Machín, M. Cotto, J. Ducongé, J. Arango, C. Morant and F. Márquez, Synthesis and characterization of Au@TiO_2 NWs and their catalytic activity by water splitting: a comparative study with Degussa P25. Am, *J. Eng. Appl. Sci.*, 2017, **10**, 298–311.
35 K. S. Babu and V. Narayanan, Hydrothermal synthesis of hydrated zinc oxide nanoparticles and its characterization, *Chem. Sci. Trans.*, 2013, **2**(S1), S33–S36.
36 M. Gholami, M. Shirzad-Siboni, M. Farzadkia and J.-K. Yang, Synthesis, characterization, and application of ZnO/TiO_2 nanocomposite for photocatalysis of a herbicide (Bentazon), *Desalin. Water Treat.*, 2016, **57**(29), 13632–13644.
37 T. Blasco, M. Camblor, A. Corma and J. Perez-Pariente, The state of Ti in titanoaluminosilicates isomorphous with zeolite. beta, *J. Am. Chem. Soc.*, 1993, **115**(25), 11806–11813.
38 F. A. Tantray, A. Agrawal, M. Gupta, J. T. Andrews and P. Sen, Effect of oxygen partial pressure on the structural and optical properties of ion beam sputtered TiO_2 thin films, *Thin Solid Films*, 2016, **619**, 86–90.
39 S. A. Ansari, M. M. Khan, M. O. Ansari and M. H. Cho, Gold nanoparticles-sensitized wide and narrow band gap TiO_2 for visible light applications: a comparative study, *New J. Chem.*, 2015, **39**(6), 4708–4715.
40 Y. Liu, J.-z. Tian, X. Hao, Y.-j. Zheng, T. Jing, Y.-p. Zhao and W.-l. Yang, Preparation of TiO_2/porous glass-H with the coupling of photocatalysis oxidation–adsorption system in the initial position and its desulfurization performance on model fuel, *RSC Adv.*, 2021, **11**(46), 28508–28520.

41 D. Qiao, Z. Li, J. Duan and X. He, Adsorption and photocatalytic degradation mechanism of magnetic graphene oxide/ZnO nanocomposites for tetracycline contaminants, *Chem. Eng. J.*, 2020, **400**, 125952.

42 L. Li, C.-G. Niu, H. Guo, J. Wang, M. Ruan, L. Zhang, C. Liang, H.-Y. Liu and Y.-Y. Yang, Efficient degradation of Levofloxacin with magnetically separable $ZnFe_2O_4$/NCDs/Ag_2CO_3 Z-scheme heterojunction photocatalyst: vis-NIR light response ability and mechanism insight, *Chem. Eng. J.*, 2020, **383**, 123192.

43 S. Meng, J. Zhang, S. Chen, S. Zhang and W. Huang, Perspective on construction of heterojunction photocatalysts and the complete utilization of photogenerated charge carriers, *Appl. Surf. Sci.*, 2019, **476**, 982–992.

44 B. Jaleh, M. Gandomi Rouzbahani, K. Abedi, S. Azizian, H. Ebrahimi, M. Nasrollahzadeh and R. S. Varma, Photocatalytic decomposition of VOCs by AC–TiO_2 and EG–TiO_2 nanocomposites, *Clean Technol. Environ. Policy*, 2019, **21**, 1259–1268.

45 Y.-C. Chan, J.-N. Chen and M.-C. Lu, Intermediate inhibition in the heterogeneous UV-catalysis using a TiO_2 suspension system, *Chemosphere*, 2001, **45**(1), 29–35.

46 Z. Lin, X. Jiang, W. Xu, F. Li, X. Chen, H. Wang, S. Liu and X. Lu, The effects of water, substrate, and intermediate adsorption on the photocatalytic decomposition of air pollutants over nano-TiO_2 photocatalysts, *Phys. Chem. Chem. Phys.*, 2024, **26**, 662–678.

47 J. Zhang, H. B. Yang, D. Zhou and B. Liu, Adsorption energy in oxygen electrocatalysis, *Chem. Rev.*, 2022, **122**(23), 17028–17072.

48 R. Nadarajan, W. A. W. A. Bakar, R. Ali and R. Ismail, Effect of structural defects towards the performance of TiO_2/SnO_2/WO_3 photocatalyst in the degradation of 1, 2-dichlorobenzene, *J. Taiwan Inst. Chem. Eng.*, 2016, **64**, 106–115.

49 Y. Zhang, Q. Shao, H. Jiang, L. Liu, M. Wu, J. Lin, J. Zhang, S. Wu, M. Dong and Z. Guo, One-step co-precipitation synthesis of novel BiOCl/CeO_2 composites with enhanced photodegradation of rhodamine B, *Inorg. Chem. Front.*, 2020, **7**(6), 1345–1361.

50 J. Tian, Q. Shao, J. Zhao, D. Pan, M. Dong, C. Jia, T. Ding, T. Wu and Z. Guo, Microwave solvothermal carboxymethyl chitosan templated synthesis of TiO_2/ZrO_2 composites toward enhanced photocatalytic degradation of Rhodamine B, *J. Colloid Interface Sci.*, 2019, **541**, 18–29.

51 X. Li, F. Li, X. Lu, S. Zuo, C. Yao and C. Ni, Development of $Bi_2W_{1-x}Mo_xO_6$/Montmorillonite nanocomposite as efficient catalyst for photocatalytic desulfurization, *J. Alloys Compd.*, 2017, **709**, 285–292.

52 X. Lu, X. Li, F. Chen, Z. Chen, J. Qian and Q. Zhang, Biotemplating synthesis of N-doped two-dimensional CeO_2–TiO_2 nanosheets with enhanced visible light photocatalytic desulfurization performance, *J. Alloys Compd.*, 2020, **815**, 152326.

53 B. Arjun Kumar, T. Elangovan, D. Karthigaimuthu, D. Aravinth, G. Ramalingam, F. Ran and S. Sangaraju, CdSe Quantum Dots Bedecked on ZnO/TiO_2/CuO Ternary Nanocomposite for Enhanced Photocatalytic and Photovoltaic Applications, *Langmuir*, 2023, **39**(45), 15864–15877.

54 V. K. Landge, C.-M. Huang, V. S. Hakke, S. H. Sonawane, S. Manickam and M.-C. Hsieh, Solar-energy-driven Cu-ZnO/TiO_2 nanocomposite photocatalyst for the rapid degradation of Congo Red azo dye, *Catalysts*, 2022, **12**(6), 605.

55 X. Zheng, D. Li, X. Li, J. Chen, C. Cao, J. Fang, J. Wang, Y. He and Y. Zheng, Construction of ZnO/TiO_2 photonic crystal heterostructures for enhanced photocatalytic properties, *Appl. Catal., B*, 2015, **168**, 408–415.